Transmission electron spin resonance in dilute rare-earth aluminum alloys*

J. F. Siebert,† S. A. Dodds,‡ and R. H. Silsbee
Laboratory of Atomic and Solid State Physics and Materials Science Center, Cornell University, Ithaca, New York 14853

(Received 20 May 1976)

We report transmission-electron-spin-resonance (TESR) measurements on dilute alloys of Er, Tm, and Lu in aluminum. We have derived theoretical expressions for the effects of the exchange and crystal-field interactions on the resonance properties of the Er and Tm alloys. A computer fit of these expressions to the data yields values for the crystal-field parameters and the sign, magnitude, and a measure of the k dependence of the exchange interaction for each alloy. Combining the TESR results with direct EPR measurements on Al:Er, we obtain the free-ion g value of Er^{3+} and a measure of the electron-electron enhancement in the host. The TESR measurements also yield the outer-shell spin-flip scattering cross sections σ_{sf} for Er, Tm, and Lu. Corresponding resistivity measurements indicate that the outer-shell scattering properties of these impurities are quite similar, in that they are all characterized by roughly the same value for the ratio σ_{sf}/ρ_r.

I. INTRODUCTION

Transmission-electron-spin resonance (TESR) is a relatively new experimental technique for observing conduction-electron spin resonance in pure metals.[1,2] Since the presence of very small amounts of impurities in the metal can significantly affect the properties of the resonance, the TESR technique has proved to be a useful probe for studying the behavior of both magnetic and nonmagnetic impurities in a metallic environment.[3-5] In particular, it provides detailed information about some of the dynamics of the spin-dependent scattering of conduction electrons by impurities in the dilute limit, where impurity-impurity interactions can be neglected for all temperatures of interest. In this paper, we report TESR and EPR measurements on aluminum containing dilute amounts (5–65 ppm) of rare-earth (RE) impurities.[6] We will show that these experiments provide useful information about the magnitude, sign, and k dependence of the exchange coupling between the conduction-electron and impurity-spin systems, the crystal-field splittings of the RE f shell due to its cubic metallic environment, and the spin-flip scattering cross sections for the *outer* electron shells of the RE ions. In addition, by combining the TESR results with direct measurement of the rare-earth EPR in Al:Er, we obtain the free-ion g value of Er and a measure of the electron-electron enhancement of the aluminum host.

Aluminum was chosen as the host material for several reasons. It behaves as a nearly-free-electron metal, so that host band-structure effects should be small. It has a strong TESR signal up to liquid-nitrogen temperature, so signal strength is reasonable over a large temperature range even in the presence of impurities. Finally, aluminum is trivalent, like the RE ions to be studied, which should minimize the electron scattering that results from charge contrast between host and impurity.

There are two primary "theoretical" problems when considering TESR in the presence of impurities. The first is understanding the observed line shape and position in order to extract the conduction-electron spin relaxation rate $1/T_2$ and the g value. The second is interpreting these results in terms of some more or less detailed microscopic model. For the case of nonmagnetic impurities this procedure is reasonably straightforward. Assuming classical skin-depth conditions, the relationship between the observed TESR signal and $1/T_2$ has been calculated by assigning spin and momentum relaxation times to the conduction electrons, and applying Maxwell's equations to the problem of a metal slab in a radio-frequency field.[1,7] Resonance measurements of $1/T_2$ have been made for a variety of different nonmagnetic impurities in several different hosts, and have been successfully interpreted in terms of the spin-orbit interaction, which couples the spin and orbital motion of the conduction electrons when they are in the impurity cell.[8]

When the impurities are magnetic, the problems of extracting and then interpreting the resonance parameters are no longer independent, since the conduction-electron magnetization is dynamically coupled to the local-moment magnetization. For example, when transition-metal impurities with $g=2.0$ are dissolved in a simple metal host, the exchange coupling between the local moment of the ion and the conduction-electron spin is typically so strong that only a single combined resonance is observed.[3,9] This "bottleneck" effect considerably complicates the analysis of such systems and pre-

vents a direct determination of the coupling and spin-flip parameters.[10] Furthermore, the resonance behavior of these strongly coupled alloys has traditionally been interpreted by assuming that the exchange coupling takes the simple form $-J(\vec{r})\vec{S}\cdot\vec{s}$, where $\vec{S}$ and $\vec{s}$ represent a local-moment and conduction-electron spin, respectively, and $J(\vec{r})$ characterizes the strength and range of the exchange coupling. Basic to this model is the assumption that many-body effects are small so that the impurity retains a well-defined moment localized on the impurity site, although there is considerable experimental evidence indicating that this is not a good assumption for transition-metal impurities in metal hosts.[11]

In our experiments, we have avoided these complications by working with the non-S-state rare-earth impurities Er and Tm. Because the magnetic $4f$ shell is tightly bound and well shielded within the atom, most RE impurities in a metallic environment tend to retain well-defined magnetic moments of they type they might possess as impurity ions in a simple ionic crystal. Under these circumstances, the exchange model suggested above is expected to be a reasonably good approximation. Since the rare earth is usually characterized by the total angular momentum J of its Hund's-rule ground state, the exchange interaction is conveniently written[12] as $-(g_J-1)J(\vec{r})\vec{J}\cdot\vec{s}$, where g_J is the Landé factor.

The $(2J+1)$-fold degeneracy of the ground state is partially lifted by the cubic crystal field of the aluminum host. We find that Al:Er has a Γ_7 doublet ground state[13] that is resonant at $g\cong 6.8$, while the ground state of Al:Tm is determined by our experiments to be a nonmagnetic singlet. These alloys are therefore unbottlenecked, in the sense that the effects of coupling are expected to be rather small, and can be treated in a molecular-field approximation. The first-order effect of the exchange coupling between the RE ions and the conduction-electron spins of the host is a temperature- and crystal-field-dependent shift and broadening of the TESR signal. This occurs because the magnetic moment, and therefore the exchange scattering, depend on the thermal occupation of the ionic energy levels of the RE f shell, as determined by the crystal fields. Consequently, our TESR results provide information about crystal-field splittings, as well as information about the exchange coupling.

In this weak-coupling regime, temperature-independent contributions to the conduction-electron spin relaxation rate due to nonmagnetic spin-orbit scattering in the outer shells of the RE ions are simply additive, and can be easily separated from the f-shell contributions. To facilitate this separation, we have made corresponding TESR measurements on Al:Lu. This is the ideal nonmagnetic reference alloy, since Lu has a full f shell, and is expected to have an outer-shell electron configuration similar to that of Er and Tm.

For these unbottlenecked systems, the procedure for determining the conduction-electron spin relaxation rate from the TESR line shape is the same as for alloys containing nonmagnetic impurities.[1,7] For this purpose, Dunifer's[14] calculations and charts are very helpful, and have been used to extract the parameters presented here. In interpreting our results, we have used the exchange model described above and first-order perturbation theory to derive expressions for the exchange contributions to the TESR g value and linewidth as a function of temperature, impurity concentration, crystal-field parameters, and electron-electron enhancement of the host. Comparisons between computer calculations of these expressions and our data provide reasonable agreement between theory and experiment.

The paper is organized as follows. Section II contains a brief description of the TESR experimental apparatus and the methods used to prepare and analyze the samples. Section III is a presentation of the perturbation theory for the impurity-induced spin-lattice relaxation and resonance g shift due to the exchange coupling assumed above, but modified to include the effects of crystal-field splitting and electron-electron enhancement. Section IV is a presentation and comparison with theory of the experimental results. Section V summarizes and gives our conclusions.

II. EXPERIMENTAL TECHNIQUE

A. Apparatus

The TESR technique has been fully described elsewhere[1,3,14] as has the particular spectrometer used for these experiments.[15] Briefly, the measurements were carried out at X band with a single-klystron 30-MHz superheterodyne spectrometer using a tunnel-diode microwave preamplifier to give a system noise figure of 9 dB, or a sensitivity of 3×10^{-20} W at a one-cycle bandwidth. Because of this high sensitivity, it is necessary to maintain more than 180-dB isolation between the transmitter and receiver cavities in order to obtain useful data at the maximum available incident power of about 100 mW.

The cavity assembly consists of two cylindrical microwave cavities, operating in TE_{111} modes, and arranged symmetrically with the sample forming a common end wall. Single-crystal sapphire disks greased onto the sample surfaces act to support the sample (typically 0.05 mm thick), concen-

trate the microwave magnetic field at the sample, shorten the cavities, and improve the thermal contact between cavity and sample. Sapphire tuning rods are used to equalize the cavity frequencies during operation. A central "sandwich" of copper-plated brass flanges containing the sample and sapphire disks is removable as a unit, and is sealed to the otherwise rigid cavity assembly using indium gaskets. A spiral ridge was machined onto the flange surfaces in contact with the sample to produce a cold-weld seal consistent with the requirement of more than 180-dB isolation between the cavities.

In operation, the cavities are sealed in an exchange-gas–isolation can, and using conventional procedures the TESR can be run at temperatures from 1.7 °K to above liquid-nitrogen temperature. A calibrated GaAs diode attached to the cavity is used to measure the absolute temperature. Independent measurements have established that the temperature difference between this sensor and the sample center is less than 0.5 °K at high temperature and maximum microwave power, and is much smaller at the low microwave powers used below 5 °K.

B. Sample preparation

Since the solid solubility of the rare earths in aluminum is very low, and because they oxidize readily during the conventional successive dilution, rolling, and annealing procedures used to make dilute alloy foils, it was necessary to develop a one-step method for preparing samples directly in the form of foils at the desired impurity concentrations. The technique used is a variant of "getter sputtering," which is known to produce thin films of high purity.[16,17] The essential feature of this method is that it utilizes the high reactivity of the sputtering material as a pump or "getter" to reduce the reactive gas partial pressure in the vicinity of the sample to a negligible level during the sample preparation. This can be achieved in a conventional oil-diffusion-pumped vacuum system provided an inner "getter-sputtering" enclosure is employed to control the *local* reactive gas partial pressure.

The apparatus used here consists of a conventional 10^{-6}-Torr bell-jar vacuum system where the main chamber contains the sample preparation assembly shown schematically in Fig. 1. The top can contains two rare-earth cathodes, one for each side of the sample foil, and appropriate shields. Stainless-steel tubes soldered to the outside walls provide for liquid-nitrogen cooling during operation, insuring good gettering action. The argon sputtering gas inlets between outer and inner chambers are strategically located relative to the

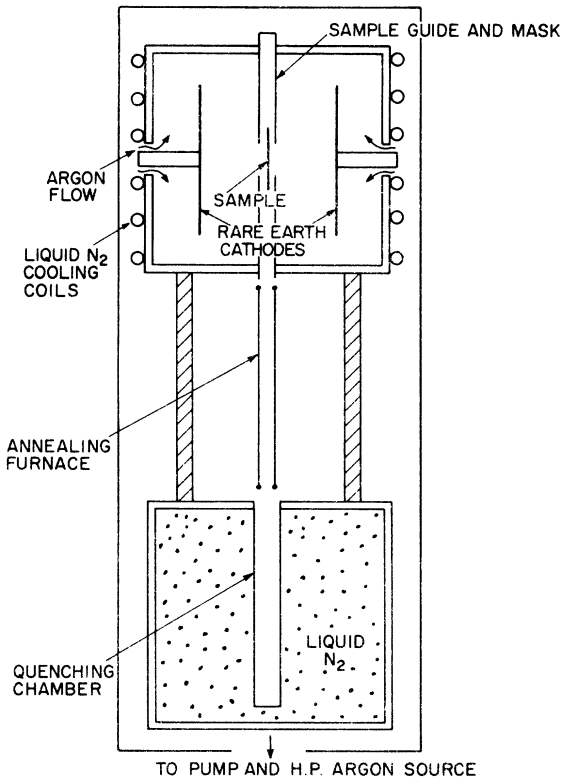

FIG. 1. Schematic diagram of the getter sputtering sample preparation apparatus. The portion shown is approximately 80 cm tall.

continuously sputtering rare-earth cathodes so that reactive gases entering with the argon react with the rare-earth vapor and are deposited on the chilled walls before reaching the sample preparation zone. The annealing furnace is two pieces of tantalum foil, supported by molybdenum strips and polycrystalline sapphire insulators. It is heated by passing a large current through the foils. The bottom can is liquid-nitrogen filled, and contains a coil for cooling the argon gas used to quench the sample after annealing. Not shown is an air lock which is used to introduce the sample foil through the top of the continuously evacuated main chamber.

In operation, liquid nitrogen is forced through the cooling lines and a flow maintained through all subsequent operations. Before preparing a sample, the furnace is outgassed by heating well above the annealing temperature, and rare earth is sputtered onto the sample chamber walls to getter the residual reactive gases. The sputtering potential is then reversed, and the natural oxide layer is sputtered off the aluminum. This step is essential since the oxide layer acts as a reactive barrier to the diffusion of the rare earth into the

foil.[17] A shield prevents contamination of the rare rare-earth cathodes during the oxide removal process. After oxide removal, an appropriate amount of rare earth is sputtered onto the bare foil, and the sample is then lowered into the tantalum furnace where it is annealed at just below the melting temperature of aluminum for a time long enough to allow the rare-earth impurities to diffuse uniformly throughout the sample. An annealing time of 90 min at 620 °C was found to give satisfactory results. During the operation the cathodes are continuously getter sputtered to prevent reactive gas contamination of the sample surface before the diffusion process is complete. Finally, the foil is quenched with a blast of cold argon gas in the bottom part of the apparatus. With the present design we are able to produce three different samples simultaneously, either with the same or differing concentrations. A major feature of the sputtering technique is that deposition rates are very stable and reproducible as long as the sputtering voltages and pressure are kept constant. We are therefore able to predict nominal concentrations in the parts per million range simply by knowing the long-term sputtering rate and the deposition times.

C. Starting materials and sample characterization

The high-purity aluminum was obtained from Brookhaven National Laboratory. After rolling to the desired thickness and annealing, it has a residual resistivity ratio at 4.2 K of 2000–3000, corrected for size effect. All specimens were polycrystalline. Rare-earth metals were obtained from Research Chemicals Corp., Phoenix, Ariz. Purity is better than 99.9% in all cases, with the dominant impurities being other rare earths and calcium.

Residual resistivity measurements at 4.2 K were used to check sample homogeneity and concentration ratios, after size-effect correction. In all cases, homogeneity was better than 10% over the area of the sample exposed to microwaves in the TESR spectrometer. Maximum concentration occurred at the center, falling smoothly toward the edges. Concentration ratios determined by resistivity agree within a few percent with ratios calculated from TESR linewidth, TESR line shift, and activation analysis.

Absolute concentrations were determined by neutron activation analysis, carried out in the Cornell University Materials Science Center Analytical Facility. Sensitivity for the rare earths is at the 0.01–1-ppm level, and the high-purity host generally eliminates interferences, so the measurement is quite straightforward. Instrumental determinations were made for all samples, by comparison with standards made from rare-earth oxides wrapped in aluminum foil. The accuracy is estimated to be ±5%.

III. THEORY

The TESR linewidth ($\Delta H = 1/\gamma T_2$) and g shift of dilute alloys are determined by contributions from both the host and the impurities. To effect a separation we will assume that the linewidth and g shift of pure aluminum present fixed and additive backgrounds in the alloys, independent of impurity type or concentration, that can be subtracted out.[4] In this way, we focus attention on ΔH_i and Δg_i, the impurity contributions to the linewidth and g shift, respectively. Furthermore, rare-earth ions are characterized by a xenonlike core of closed electron shells and a partially filled "magnetic" $4f$ shell. Since the $4f$ electrons are well shielded by $5s$, $5p$, $6s$, and possibly $5d$ electrons, the effect of the magnetic shell on the transport properties of metals containing rare-earth impurities is usually small relative to the outer-shell contributions. However, these outer-shell contributions are typically temperature independent so that we can use the temperature dependence of the magnetic contributions to make the additional separations

$$\Delta H_i(T) = \Delta H_{ex}(T) + \Delta H_{so} ,$$

$$\Delta g_i(T) = \Delta g_{ex}(T) + \Delta g_{so} ,$$

where the subscripts have been chosen to emphasize that the magnetic and outer-shell contributions can be attributed to the exchange and spin-orbit interactions, respectively.

Since the outer-shell configuration is approximately constant across the rare-earth series, we would expect the spin-orbit contributions to be roughly the same for all of the impurities considered here. Furthermore, it has been shown that Δg_{so}, the shift due to spin-orbit coupling, is only about 0.1% of the linewidth due to the same interaction.[18] For our alloys, the expected shift would be less than 1 G, and totally unmeasurable. Therefore, it is the magnetic contributions ΔH_{ex} and Δg_{ex}, and their dependence on temperature, impurity concentration, crystal-field parameters, and electron-electron enhancement of the host, that are of most interest. In this section, we present the results of a first-order perturbation-theory calculation of these contributions, assuming that the exchange coupling can be characterized by the simple isotropic model $-(g_J - 1)J(\vec{r})\vec{J}\cdot\vec{s}$ discussed in Sec. I. We also assume for the purpose of this calculation that all dynamic and bottleneck effects can be neglected. Furthermore, by restricting ourselves to lowest-order perturbation theory, we specifically exclude higher-order Kondo terms from our results. The validity and

limitations of these assumptions for the alloys studied here are discussed in Sec. IV, where a comparison between theory and the experimental data is made. Finally, because of even more restrictive approximations that must be made in order to include the effects of electron-electron enhancement, we have carried out the derivations both with and without enhancement considerations. In each case, we have also quoted the results of corresponding calculations for the effect of the exchange coupling on the linewidth and g value of the direct EPR of the rare-earth impurities.

Case A: Without enhancement

Using the above assumptions and approximations, it is shown in the Appendix that the expressions for the exchange-induced fractional change in the TESR g value and linewidth take the form

$$\frac{\Delta g_{ex}}{g_{0s}} = \frac{g_s - g_{0s}}{g_{0s}} = \left(\frac{c(g_J - 1)\langle J(\vec{k}, \vec{k})\rangle_{E_F}}{g_s \mu_B H}\right)\langle J_z\rangle , \quad (1)$$

$$\frac{\Delta H_{ex}}{H} = \left(\frac{\pi \rho c (g_J - 1)^2 \langle |J(\vec{k}, \vec{k}')|^2\rangle_{E_F}}{g_s \mu_B H}\right)\langle G\rangle , \quad (2)$$

where g_J is the Landé g factor. g_{0s} is the pure-host g value, c is the fractional impurity concentration, and ρ is the density of states per atom of conduction electrons of one spin direction at the Fermi energy. We have defined

$$J(\vec{k}, \vec{k}') \equiv N_0 \langle \vec{k}|J(\vec{r})|\vec{k}'\rangle ,$$

where N_0 is the host atomic density and the states $|\vec{k}\rangle$ are the exact one-electron states of electrons moving in the electric field of the lattice and the impurity, but neglecting the exchange and spin-orbit interactions. In each expression above the value of the k-dependent exchange energy is averaged over the Fermi surface. The dependence of the g shift and linewidth on temperature and crystal-field splittings is contained in the thermal averages

$$\langle J_z\rangle = \frac{1}{Z}\sum_a \langle a|J_z|a\rangle e^{-E_a/k_B T} , \quad (3)$$

$$\langle G\rangle = \frac{1}{Z}\sum_{a,b} |\langle b|J_+|a\rangle|^2 \frac{(E_b - E_a)/k_B T}{e^{E_b/k_B T} - e^{E_a/k_B T}} , \quad (4)$$

where $|a\rangle$ and E_a are the $2J+1$ exact eigenstates and eigenenergies of the rare-earth f shell in the presence of both the host crystal field and the external magnetic field applied in the z direction, J_+ is the angular momentum raising operator, and Z is the appropriate partition function. $\langle J_z\rangle$ is just the mean z component of the total ionic angular momentum, and, therefore, the fractional g shift can be expressed in the more familiar form[19] $\Delta g_{ex}/g_{0s} = \lambda \chi_f$, where χ_f is the dc susceptibility of the rare-earth impurities and λ is the appropriate molecular-field constant containing $\langle J(\vec{k}, \vec{k})\rangle_{E_F}$. This simple result is a consequence of our original assumption that the system is completely unbottlenecked.

Our calculation of the exchange linewidth is also similar to previous calculations of paramagnetic relaxation in metals,[20] but has been modified to include explicitly the effects of crystal-field splitting and the finite range of the exchange coupling. Therefore, $\langle G\rangle$ is just the thermally weighted sum of the exchange-induced spin-flip transition probabilities between the crystal-field eigenstates of the rare-earth impurities. In the high-temperature limit, $\langle G\rangle$ saturates at $\frac{2}{3}J(J+1)$, and Eq. (2) reduces to the usual form for exchange scattering from a degenerate multiplet.[21]

Note that the temperature dependences of Eqs. (1) and (2) are determined entirely by the properties of the crystal field, since the exchange parameters enter these expressions only as temperature-independent scale factors. Therefore, the crystal-field and exchange parameters can be separately determined from the shape and from the scale of these temperatures dependences, respectively. It should also be noted that the only requirement for observable temperature dependences of ΔH_{ex} and Δg_{ex} is that the impurity ions have magnetically coupled low-lying crystal-field levels that can be thermally populated at the temperatures of interest. Consequently, the TESR technique can be used to determine exchange and crystal-field parameters for ions with either magnetic or nonmagnetic ground states, as long as this condition is satisfied.

Finally, when it is possible to observe directly the rare-earth resonance, as in the case of Al:Er, this second resonance is also characterized by exchange-induced contributions to the g value and linewidth, which in general depend upon the details of the crystal-field splittings as well as on the exchange coupling.[22] However, by restricting our EPR measurements to the temperature regime $g_f \mu_B H \ll k_B T \ll \Delta$, where Δ is the isolation energy between the ground and first excited states of the impurity, the effects of higher crystal-field multiplets on the resonance are experimentally unobservable. In this regime, the theoretical expressions for the exchange-induced g shift and thermal broadening of the linewidth are those appropriate to an isolated ground state and take the simple forms[13]

$$\Delta g_f = (g_f - g_{0f}) = g_{0f}\left(\frac{g_J - 1}{g_J}\right)\rho\langle J(\vec{k}, \vec{k})\rangle_{E_F} , \quad (5)$$

$$b = \frac{\partial \Delta H_f}{\partial T} = g_{0f}\frac{\pi k_B}{\mu_B}\left(\frac{g_J - 1}{g_J}\right)^2 \rho^2 \langle |J(\vec{k}, \vec{k}')|^2\rangle_{E_F} , \quad (6)$$

where g_{0f} is the free-ion g value of the rare-earth impurities.

Note that a careful experimental determination of the properties of both resonances as well as a determination of the rare-earth impurity concentration leave us with four equations in the three unknowns $\langle J(\vec{k},\vec{k})\rangle_{E_F}$, $\langle|J(\vec{k},\vec{k}')|^2\rangle_{E_F}$, and g_{0f}, and, hence, with the opportunity to check the self-consistency of our theoretical analysis. Indeed, we will show that our data on Al:Er do suggest an inconsistency, and therefore the need for a more sophisticated theoretical treatment.

Case B: With enhancement

Of the several possible explanations for the inconsistency suggested above, our neglect of electron-electron enhancement of the host magnetic susceptibility seems the most reasonable. It is well known that the Coulomb interaction between conduction electrons produces collective effects that act to enhance the Pauli susceptibility, and therefore can affect the behavior of any system that involves either directly or indirectly the electron gas.[23,24] Calculations of these effects on EPR and TESR measurements have been made,[25] but only with the rather restrictive assumptions of a spherical moment and Fermi surface, and an electron-electron interaction range that is either zero or infinite. In this approximation, both the electron-electron and electron-moment exchange-coupling matrix elements are at most functions of the wave-vector difference $\vec{q}=\vec{k}'-\vec{k}$ between incident and scattered electrons, and the resulting modified expressions for Eqs. (1) and (2) are

$$\frac{\Delta g_{ex}}{g_{0s}}=\left(\frac{c(g_J-1)J(0)}{g_s\mu_B H}\right)\langle J_z\rangle\ , \tag{7}$$

$$\frac{\Delta H_{ex}}{H}=\left(\frac{\pi\rho c(g_J-1)^2\langle J(\vec{q})^2\eta(\vec{q})^2\rangle_{E_F}}{g_s\mu_B H\eta(0)}\right)\langle G\rangle\ , \tag{8}$$

where $J(\vec{q})=N_0(\vec{k}|J(\vec{r})|\vec{k}+\vec{q})$. $\eta(\vec{q})$, equal to one for $\vec{q}\neq 0$ in the infinite-range limit, is the host susceptibility enhancement factor [$\eta(0)$ is the usual Stoner factor] and we have assumed that the enhancement $[\eta(\vec{q})]^2/\eta(0)$ calculated by Zitkova-Wilcox[25] is appropriate for terms off-diagonal in the crystal-field levels as well as for the diagonal terms. Corresponding expressions for the EPR g shift and thermal broadening are

$$\Delta g_f=g_{0f}\left(\frac{g_J-1}{g_J}\right)\rho J(0)\eta(0)\ , \tag{9}$$

$$b=g_{0f}\frac{\pi k_B}{\mu_B}\left(\frac{g_J-1}{g_J}\right)^2\rho^2\langle J(\vec{q})^2\eta(\vec{q})^2\rangle_{E_F}\ . \tag{10}$$

Note that both the TESR and EPR linewidths include identical averages over the wave vector $\vec{q}$ spanning the Fermi surface. However, the TESR linewidth is deenhanced by the Stoner factor as a result of conduction-electron spin relaxation to the self-consistently-enhanced instantaneous local field.[25]

Therefore, in this model TESR and EPR measurements on alloys containing impurities with a ground-state resonance can be used to make self-consistent determination of the four enhancement modified parameters $J(0)$, $\langle J(\vec{q})^2\eta(\vec{q})^2\rangle_{E_F}$, g_{0f}, and $\eta(0)$ contained in Eqs. (7)–(10). To obtain a direct estimate of $\langle J(\vec{q})^2\rangle_{E_F}^{1/2}$ it will be necessary to make further approximations and also to refer to NMR measurements on pure aluminum that provide additional information about the $\vec{q}$ dependence of the host enhancement factor.

IV. EXPERIMENTAL RESULTS AND ANALYSIS

A. Exchange and crystal-field parameters

Data points giving the temperature dependence of the impurity-induced g shift and linewidth for various Er and Tm concentrations are shown in Figs. 2–5, together with some theoretically fitted curves.[26] These curves represent Eqs. (1) and (2), and are the result of a computer program designed

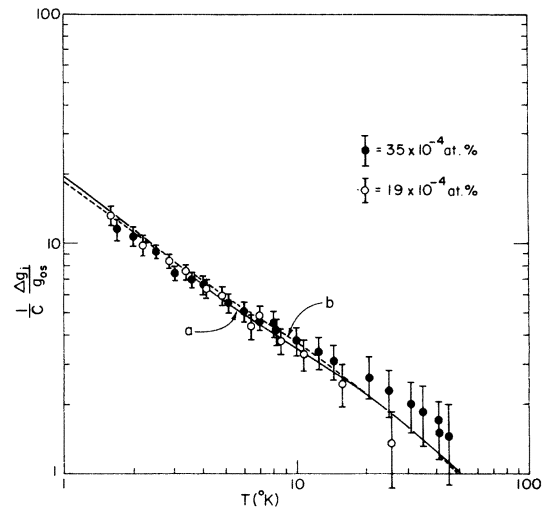

FIG. 2. Temperature dependence of the impurity-induced TESR fractional g shift $\Delta g_i/g_{0s}$ per Er impurity concentration c (expressed in at.%). Within experimental error, measurements at $c=5\times10^{-4}$ at.% yield identical behavior. The solid lines in Figs. 2–5 are the theoretical fits to the data used to determine the parameter values listed in Table I, as described in the text. The dashed lines show the effect on the fits and on the values of the exchange parameters for different values of the ground-state isolation energy Δ. All measurements were made at 9.2 GHz and referenced to the pure-Al g value $g_{os}=1.997$ (Ref. 26). (a) $\Delta=45$ K, $\langle J(\vec{k},\vec{k})\rangle_{E_F}=0.19$ eV; (b) $\Delta=30$ K, $\langle J(\vec{k},\vec{k})\rangle_{E_F}=0.18$ eV.

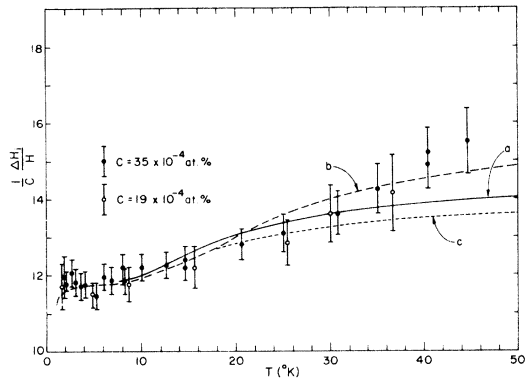

FIG. 3. Temperature dependence of the impurity contribution to the TESR fractional linewidth $\Delta H_i/H$ (where $\Delta H_i \equiv 1/\gamma T_2$) per Er impurity concentration c (expressed in at.%), where H is the measured resonance field. The background linewidth of pure Al over this temperature range (Ref. 26) was assumed to be additive and subtracted out. The solid and dashed curves are explained in Fig. 2. The dotted curve (c) shows the effect on the value of $\langle|J(\vec{k},\vec{k}')|^2\rangle^{1/2}_{E_F}$ when the low-temperature data is emphasized in making the theoretical fit, as discussed in the text. (a) $\Delta = 45$ K, $\langle|J(\vec{k},\vec{k}')|^2\rangle^{1/2}_{E_F} = 0.13$ eV; (b) $\Delta = 60$ K, $\langle|J(\vec{k},\vec{k}')|^2\rangle^{1/2}_{E_F} = 0.155$ eV; (c) $\Delta = 45$ K, $\langle|J(\vec{k},\vec{k}')|^2\rangle^{1/2}_{E_F} = 0.115$ eV.

to evaluate $\langle J_z\rangle$ and $\langle G\rangle$ as a function of temperature, using the exact crystal-field eigenstates and eigenvalues of the rare-earth f shell in the presence of an external magnetic field. For the cubic crystal-field Hamiltonian we have used the operator equivalent form of Lea, Leask, and Wolf[27]

$$H = W[(O_4/F_4)x + (1-|x|)(O_6/F_6)] + g_J \mu_B(\vec{H}\cdot\vec{J}), \tag{11}$$

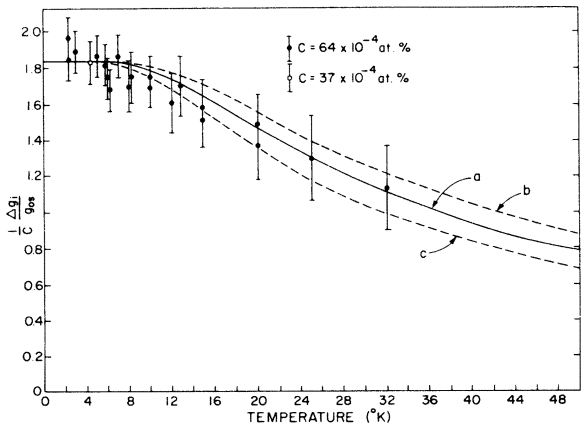

FIG. 4. Temperature dependence of the impurity-induced TESR fractional g shift $\Delta g_i/g_{0s}$ per Tm impurity concentration c (expressed in at.%). (a) $\Delta = 35$ K, $\langle J(\vec{k},\vec{k})\rangle_{E_F} = 0.30$ eV; (b) $\Delta = 40$ K, $\langle J(\vec{k},\vec{k})\rangle_{E_F} = 0.34$ eV; (c) $\Delta = 30$ K, $\langle J(\vec{k},\vec{k})\rangle_{E_F} = 0.26$ eV.

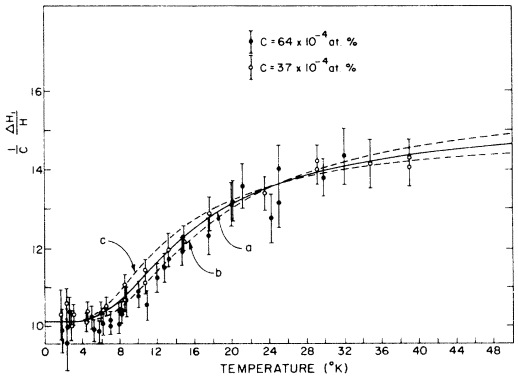

FIG. 5. Temperature dependence of the impurity contribution to the TESR fractional linewidth $\Delta H_i/H$ (where $\Delta H_i = 1/\gamma T_2$) per Tm impurity concentration c (expressed in at.%), where H is the measured resonance field. (a) $\Delta = 35$ K, $\langle|J(\vec{k},\vec{k}')|^2\rangle^{1/2}_{E_F} = 0.195$ eV; (b) $\Delta = 40$ K, $\langle|J(\vec{k},\vec{k}')|^2\rangle^{1/2}_{E_F} = 0.205$ eV; (c) $\Delta = 30$ K, $\langle|J(\vec{k},\vec{k}')|^2\rangle^{1/2}_{E_F} = 0.185$ eV.

where O_4 and O_6 are fourth- and sixth-order angular momentum operators whose exact forms depend on the direction of the field $\vec{H}$ with respect to the crystal-field axes,[28] and F_4 and F_6 are numbers listed by them characteristic of the rare-earth f-shell ground state. W is an energy scale factor, here expressed in degrees Kelvin, and x is a parameter that ranges from -1 to 1.

For both alloys, the solid lines in the figures give the best simultaneous theoretical fits to the g-shift and linewidth data. As noted earlier, the shapes and horizontal scale factors are determined principally by the crystal-field parameters x and W, while the vertical scales are determined principally by the two exchange averages. This allows us to determine both exchange and crystal-field parameters. Our results are listed in Table I, along with values for other experimental parameters whose determination will be discussed later. At the moment we wish to make the following comments about the computer fits shown and the resulting values for the exchange and crystal-field parameters.

1. Computer fits and dynamic coupling contributions

The solid-line computer fits to the experimental data are acceptable over the entire measured temperature range for Al:Tm. For Al:Er it was possible to make measurements at somewhat higher temperatures, and deviations from the fitted curves are seen. We suggest that these high-temperature deviations can be attributed to our neglect of dynamic or bottlenecking effects[21] in applying Eqs. (1) and (2) to systems like Al:Er, where the im-

TABLE I. Comparison of parameters characterizing the crystal-field, exchange, and transport properties of various rare-earth impurities in aluminum.

Rare-earth ion	Ground state	Crystal-field parameters			Exchange averages (eV)		Transport properties	
		W (°K)	x	Δ (°K)	$\langle J(\vec{k},\vec{k})\rangle_{E_F}$	$\langle\lvert J(\vec{k},\vec{k})\rvert^2\rangle^{1/2}_{E_F}$	ρ_r ($\mu\Omega$ cm/at.%)	σ_{sf} (10^{-18} cm^2)
Er^{3+}	Γ_7	+0.6	−0.3	45 ± 20	0.19 ± 0.02	0.13 ± 0.03	3.6 ± 0.25	4.7 ± 0.7
Tm^{3+}	Γ_2	−0.75	+0.5	35 ± 10	0.30 ± 0.05	0.195 ± 0.03	3.6 ± 0.25	4.9 ± 0.25
Lu^{3+}	•••	•••		•••	•••	•••	4.6 ± 0.4	5.9 ± 0.4

purities have a ground-state resonance. In this situation, our assumption of an unbottlenecked system is reasonable only as long as the frequency separation between the rare-earth and conduction-electron spin resonances is much larger than the cross-relaxation rate $1/T_{fs}$ between them. Since $1/T_{fs}$ increases in direct proportion to the temperature,[22] our neglect of dynamic coupling at higher temperatures may not be justified.

To obtain a rough estimate of the effects of an incipient bottleneck on our results, we approximate the resonance properties of the Er and conduction-electron spin systems by the two exchange-coupled Bloch-like equations first proposed by Hasegawa,[21] which have been extended to include the case of different g values and relaxation to equilibrium in the instantaneous field,[29]

$$\frac{d\vec{M}_s}{dt} = \gamma_s \vec{M}_s \times (\vec{H} + \lambda \vec{M}_f) - \left(\frac{1}{T_{s1}} + \frac{1}{T_{sf}}\right)\delta\vec{M}_s + \left(\frac{\gamma_s}{\gamma_f}\right)\left(\frac{1}{T_{fs}}\right)\delta\vec{M}_f \,, \tag{12}$$

$$\frac{d\vec{M}_f}{dt} = \gamma_f \vec{M}_f \times (\vec{H} + \lambda \vec{M}_s) - \left(\frac{1}{T_{f1}} + \frac{1}{T_{fs}}\right)\delta\vec{M}_f + \left(\frac{\gamma_f}{\gamma_s}\right)\left(\frac{1}{T_{sf}}\right)\delta\vec{M}_s \,. \tag{13}$$

$\vec{M}_s$ and $\vec{M}_f$ are the conduction-electron and rare-earth magnetizations, respectively, γ_s and γ_f are the corresponding gyromagnetic ratios, T_{s1} and T_{f1} are the corresponding relaxation times to the lattice, T_{sf} and T_{fs} are the cross-relaxation times, and $\delta\vec{M}_s$ and $\delta\vec{M}_f$ are the deviations of each magnetization from equilibrium in their instantaneous fields. Focusing attention on the resonance frequency of the conduction-electron-spin-resonance signal, the solution of these equations predicts the temperature- and concentration-dependent g shift

$$\Delta g/g_{0s} \cong [\omega_s(\omega_f - \omega_s)]^{-1}[T_{sf}T_{fs}]^{-1} \,, \tag{14}$$

in *addition* to the molecular-field contribution $\lambda\chi_f$ of Eq. (1), where ω_f and ω_s are the rare-earth and conduction-electron spin resonance frequencies in the absence of the exchange coupling. Extrapolating our experimental values for the Korringa and the Overhauser relaxation rates for the isolated doublet to 50 °K, we obtain $(1/c)(\Delta g/g_{0s}) \cong 0.4$.

Our calculations also predict small but significant dynamic modifications to the conduction-electron-spin-resonance linewidth and line shape at higher temperatures. However, quantitative estimates of these effects are of questionable value, since in this rough analysis we have treated the rare-earth spin system as an isolated doublet at all temperatures, and have also ignored the effects of electron diffusion. More exact calculations,[30] taking into account the higher crystal-field levels, confirm the qualitative predictions of our simple model, although the magnitudes of the effects are reduced somewhat. In view of these difficulties at high temperature, we have chosen to emphasize the lower-temperature part (below 40 K) of the data in fitting Eqs. (1) and (2), and the solid lines express this choice. An even stronger emphasis on the low-temperature Al:Er data is shown by the dotted curve in Fig. 3, and corresponds to $\langle|J(\vec{k},\vec{k}')|^2\rangle^{1/2}_{E_F} \cong 0.115$ eV. Note that this value falls within the error bars of the value for $\langle|J(\vec{k},\vec{k}')|^2\rangle^{1/2}_{E_F}$ given in Table I.

2. *Crystal-field parameters*

Crystal-field effects on the g shift and linewidth-versus-temperature curves are not dramatic enough to permit an unambiguous determination of the crystal-field parameters W and x. Instead, it is the ground-state isolation energy Δ that proves to be the most sensitive parameter in determining the fit. The effects of different values of Δ on curve shape are illustrated by the dashed lines in Figs. 2–5. For example, the values $\Delta = 30$ and 60 °K were found to give the best fits to the Er g-shift and linewidth data, respectively. However, the solid-line curves corresponding to the single value $\Delta = 45$ °K give the best simultaneous fits to the data. Our determination that $\Delta_{Er} = 45 \pm 20$ °K, is the result of these considerations. The Al:Er fitting problems, which we have suggested are associated with an incipient bottleneck, are apparent-

ly not present in Al:Tm. This may be due to the fact that, according to our experiments, the Tm impurities have a singlet and therefore nonresonant ground state. We obtain the more accurately defined value for the ground-state isolation energy $\Delta_{\mathrm{Tm}}=35\pm 10\ ^{\circ}\mathrm{K}$.

As is usually the case for systems with cubic symmetry,[31] the problem of determining unambiguous values for the parameters W and x is considerably more difficult. For example, the observed rare-earth resonance in Al:Er requires a Γ_7 ground state, and therefore that $|x|<0.6$. However, *any* value of x in this range will provide an equally good fit as long as W is chosen to keep the ground-state isolation energy constant. Similarly, our data on Al:Tm do not completely rule out all values of x corresponding to a Γ_1 (singlet) or Γ_3 (nonmagnetic doublet) ground state, although the computer fit is most satisfactory for the Γ_2 ground state. Some of this ambiguity can be resolved by requiring reasonable consistency in the properties of the crystal-field parameters of different rare-earth impurities within the same host material. The ground states and "best" values for W and x listed in Table I are the result of this type of reasoning. Fortunately, this last assumption is not crucial to the rest of our analysis, since an accurate knowledge of values for W and x is not necessary for determining the values of the other parameters listed in the table. However, it is still interesting to note that a point-charge model of the crystal field[27] predicts signs for the values of x opposite to the ones that we have chosen. In this respect our results are identical to those determined from susceptibility measurements on rare-earth impurities in noble-metal hosts, where it has been suggested that the presence of a nonmagnetic $5d$ virtual bound screening state and its effect on the crystal-field potential could account for this apparent sign contradiction.[31]

3. *Exchange parameters*

The scales of the computer fits to the experimental data were used to determine the values listed for the two measures of the strength of the exchange interaction contained in Eqs. (1) and (2). There are small but significant differences between these two exchange averages for each alloy. The differences are best illustrated by the ratio $\langle J(\vec{k},\vec{k})\rangle_{E_F}/\langle|J(\vec{k},\vec{k}')|^2\rangle_{E_F}^{1/2}$, since in this form some of the experimental and fitting uncertainties cancel out. Within experimental error, both alloys are characterized by the same exchange ratio 1.5 ± 0.3. This value is comfortably consistent with the suggestion[32] that only the first few terms in the partial-wave expansion,

$$J(\vec{k},\vec{k}')=\sum_L (2L+1)P_L(\vec{k},\vec{k}')J_L\ ,$$

should be important.

This is in contrast with similar measurements of RE impurities in a silver host[5,33] which yield much higher exchange ratios, ranging from 2 to 3. On the basis of these larger values, it has been suggested that theoretical models beyond the $J(\vec{k},\vec{k}')\vec{S}\cdot\vec{s}$ Hamiltonian should be considered.[5] However since host susceptibility enhancement may be a bigger effect in Ag than Al,[24] a self-consistent analysis of the ESR and TESR data, as done below for Al, may significantly influence these conclusions. Another possibility is that the first-order perturbation-theory treatment of the $J(\vec{k},\vec{k}')\vec{S}\cdot\vec{s}$ Hamiltonian is inadequate, and that higher-order terms might be important. For example, it has been shown that calculations to the next higher order in $J\rho$ predict a suppression of the Korringa rate [Eq. (6)] in positive exchange systems.[34] Since the values of $\langle|J(k,k')|^2\rangle_{E_F}^{1/2}$ for the silver host alloys were determined from EPR measurements of the Korringa rate, such a suppression would act to increase the apparent exchange ratio observed in these experiments. In any case, arguments posed for the explanation of silver results must also be consistent with the smaller exchange ratio measured in the case of the aluminum host.

B. Free-ion g value and enhancement in Al:Er

We have made direct EPR measurements of the g value and thermal broadening of the RE resonance in Al:Er at temperatures between 1 and 4 °K, and find $g_f=6.805\pm 0.01$ and $b=10.5\pm 1.5$ G/°K.[35] Combining these results with the exchange averages obtained from the TESR measurements into Eqs. (5) and (6) leaves us with two equations in the one unknown g_{0f}, the rare-earth g value in the absence of exchange. Because of this, the value of g_{0f} can be determined in several different ways, and will be unique only if our theoretical treatment is self-consistent. For reasons to be given below, we choose to combine Eqs. (5) and (6) to form the ratio

$$\frac{g_f-g_{0f}}{b}=\frac{\mu_B}{\pi k_B\rho}\ \frac{g_J}{g_J-1}\ \frac{\langle J(\vec{k},\vec{k})\rangle_{E_F}}{\langle|J(\vec{k},\vec{k}')|^2\rangle_{E_F}}\ , \qquad (15)$$

and obtain $g_{0f}=6.735\pm 0.03$. This result is to be compared with the theoretical g value for the Er Γ_7 ground state of 6.77, which has been corrected for the breakdown of Russell-Saunders coupling in the free atom, but does not take into account perturbations of the ground-state angular momentum caused by the host, such as those due to covalent bonding or the crystal-field admixture of excited states.[36] Since both of these effects act to reduce

the g value, the slightly smaller experimental value for g_{0f} is not surprising.

It should now be noted that g_{0f}, as determined by Eq. (15), is significantly different from that predicted by the Knight-shift expression, Eq. (5). Similarly, the TESR result for $\langle|J(\vec{k},\vec{k}')|^2\rangle_{E_F}^{1/2}$ is not the same as that obtained by plugging the EPR results into Eq. (6). To explain our choice of Eq. (15) and to resolve these inconsistencies, we have reanalyzed our data in terms of the alternate set of Eqs. (7)–(10), which include electron-electron enhancement of the host. We find that the computer fits of Eqs. (7) and (8) to the data leave the value for $\langle J(\vec{k},\vec{k})\rangle_{E_F}=J(0)$ unchanged, but $\langle J(\vec{q})^2\rangle_{E_F}^{1/2}$ is now determined by the equation

$$\langle J(\vec{q})^2\eta(\vec{q})^2\rangle_{E_F}^{1/2}/[\eta(0)]^{1/2}=0.13\pm0.03\ \text{eV}, \qquad (16)$$

where the $\vec{q}$ notation has been used to emphasize that this analysis is based on the spherical-model approximation. Combining this result and the EPR results into Eq. (10) then yields the experimental value for the Stoner factor $\eta(0)=1.5\pm0.5$.

Note that modification of Eq. (15) to include enhancement does not alter the numerical value obtained for g_{0f}. This is because the exchange averages obtained from the TESR data, $J(0)$ and Eq. (16), contain the enhancement factors in just the appropriate manner to leave unaltered the numerical relationships in a modified Eq. (15). It is for this reason that we consider Eq. (15) a better choice than Eq. (5) for determining g_{0f} when enhancement is not included. Consequently, the inclusion of electron-electron enhancement can be used to resolve the inconsistency of our previous analysis and to determine the host susceptibility enhancement factor, but produces no changes in the values of the parameters listed in Table I, except for $\langle|J(\vec{k},\vec{k}')|^2\rangle_{E_F}^{1/2}$.

The separation of Eq. (16) to obtain a specific value for $\langle J(\vec{q})^2\rangle_{E_F}^{1/2}$ requires further approximations and experimental data. In particular, NMR measurements on pure aluminum show that $\langle\eta(\vec{q})\rangle_{E_F}^2/[\eta(0)]^2\cong0.83$,[37] a number that is consistent with the value 1.5 for the Stoner factor if we assume a δ-function Coulomb-interaction range between the electrons in the spherical-model approximation.[24] Furthermore, this result and a partial-wave expansion of the product $\langle J(\vec{q})^2\eta(\vec{q})^2\rangle_{E_F}$ can be used to show that the approximation $\langle J(\vec{q})^2\eta(\vec{q})^2\rangle_{E_F}\cong\langle J(\vec{q})^2\rangle_{E_F}\langle\eta(\vec{q})^2\rangle_{E_F}$ results in a less than 10% overestimate of the value of $\langle J(\vec{q})^2\rangle_{E_F}^{1/2}$ in an aluminum host.[38] Using this result, the NMR result, and our experimental results, we obtain $\langle J(\vec{q})^2\rangle^{1/2}=0.115$ eV. Therefore, the reduction in the second exchange average is less than 15%, a small effect relative to the experimental and theoretical uncertainties involved in this analysis. We conclude that our determination of the effects of enhancement are qualitatively useful in that they resolve some ambiguities and establish the sensitivity of the various parameters to enhancement, but they do not have a significant quantitative effect on our results.

C. Outer-shell transport properties

In addition to the exchange scattering by the f shell, there is spin-orbit scattering by the outer electronic shells of the rare-earth impurities. This additional scattering produces the temperature-independent contribution to the linewidth ΔH_{so} which, for purposes of comparison, is usually expressed as the spin-flip scattering cross section $\sigma_{sf}=(2\pi f/cN_0V_F)(\Delta H_{so}/H)$, where V_F is the Fermi velocity for aluminum and "f" is the microwave frequency.[39] Our values for σ_{sf} for Er, Tm and Lu impurities in aluminum are listed in the table, where the associated uncertainties are determined in part by the difficulty in separating the outer shell from the f-shell contributions to the TESR linewidth. This separation is straightforward in Al:Tm, since the f shell of Tm has a nonmagnetic singlet ground state that does not contribute to the linewidth at the lowest temperatures. Consequently, the uncertainty in σ_{sf} for Tm impurities is determined only by the uncertainties in our measurements of the low-temperature linewidths and impurity concentrations. This should also be the case in determining σ_{sf} for Lu impurities, since a full f shell will not contribute to the spin scattering at any temperature. As expected, TESR measurements on[40] Al:Lu show that the impurity contribution to the linewidth is temperature independent, and we have therefore treated it as a direct measure of ΔH_{so} in calculating the corresponding cross section. Conversely, the determination of σ_{sf} in Al:Er is more complicated, since the Er f shell has a magnetic ground state that contributes to the spin scattering at all temperatures. Therefore, the separation of the f-shell from the outer-shell contributions to the linewidth requires knowledge of $\langle|J(\vec{k},\vec{k}')|^2\rangle_{E_F}^{1/2}$, and the larger uncertainty in the value of σ_{sf} for Er reflects this additional difficulty in determining ΔH_{so}.

Also listed in the table are our measurements of the impurity contributions to the resistivities ρ_r of these alloys. These resistivity results are also a direct measure of the outer-shell electron scattering, since f-shell spin-disorder scattering contributions to the resistivity[41] are negligible in these alloys. Therefore, a convenient parameter for characterizing the outer-shell scattering properties of these impurities is the ratio σ_{sf}/ρ_r, which

is insensitive to impurity concentration. Within experimental error, all of these alloys can be characterized by the same number 1.3 ± 0.2, where the units of this ratio are determined by those of σ_{sf} and ρ_r listed in Table I. Since it is reasonable to expect that the outer-shell scattering properties of the heavy rare earths would be similar, especially when expressed in terms of this ratio, this consistency is reassuring.

V. SUMMARY

We have found that the resonance and relaxation properties of aluminum containing dilute amounts of Er or Tm can be understood by assuming the RE ions to be in well-defined (trivalent) charge states, with the magnetic $4f$ cores influenced by the host cubic crystalline field and coupled to the conduction-electron spins via the isotropic exchange interaction $-(g_J - 1)J(\vec{r})\vec{S}\cdot\vec{s}$. Applying a first-order perturbation theory of this model to our TESR results yields reasonable values for the crystal-field and exchange parameters characterizing each alloy. These experiments are applicable to impurity ions with either magnetic (Er^{3+}) or nonmagnetic ground states (Tm^{3+}), as long as they have low-lying crystal-field levels that can be thermally populated over the experimentally available temperature range. However, a magnetic ground state permits the direct observation of the RE resonance, and we have combined the results of EPR and TESR measurements on Al:Er to determine the free-ion g value of Er^{3+} and the electron-electron enhancement of the host. To reduce the uncertainties in the values of these last two parameters, it is felt that a more careful experimental study of this system along with a theoretical analysis extended to include the effects of dynamic coupling between the two resonances is necessary. Finally, the TESR and resistivity measurements on Er^{3+}, Tm^{3+}, and Lu^{3+} impurities in aluminum indicate that their outer-shell scattering properties are quite similar.

ACKNOWLEDGMENTS

The authors wish to thank Dr. M. A. Huisjen for his contributions to the design and construction of the TESR apparatus. We also wish to acknowledge valuable discussions with Professor J. Wilkins, Professor A. Portis, Dr. S. Wang, and, in particular, with Professor R. Orbach, who pointed out some omissions in our original theoretical treatment of this work. One of us (JFS) would like to thank the National Science Foundation for support during a summer when part of this work was performed.

APPENDIX: CALCULATION OF THE TESR g VALUE AND LINEWIDTH

The text expression for the exchange-induced TESR g shift is the result of trivial modifications to the conventional Knight-shift calculation,[42] and does not require further substantiation. On the other hand, our calculation of the exchange contribution to the TESR linewidth, although a generalization of Overhauser's treatment[20] of paramagnetic relaxation in metals due to scattering by nuclear spins, requires further clarification since it involves scattering by spatially extended moments experiencing a crystal field.

Therefore, consider a metal containing n conduction electrons and N rare-earth impurities per unit volume placed in a constant magnetic field H whose direction shall be called "+." We characterize the state of the conduction electrons by the spin population difference $D = n_- - n_+$, which in thermal equilibrium has the value D_0 proportional to the applied magnetic field. We further assume that initially there is a nonequilibrium spin population difference $D - D_0$, whose return to equilibrium can be described by the equation[20]

$$\frac{dD}{dt} = -\frac{D - D_0}{T_1}, \tag{A1}$$

where T_1 is the spin-lattice relaxation time. Alternatively, the return to equilibrium can be expressed as an appropriately weighted sum over initial and final states of the microscopic transition rate

$$W_{ab}(\vec{k}+, \vec{k}'-) = (2\pi/\hbar)|\langle b\vec{k}'-|V|a\vec{k}+\rangle|^2 \delta(E_a + E_{\vec{k}+} - E_b - E_{\vec{k}'-}), \tag{A2}$$

which gives the probability that the impurity interaction "V" scatters an electron from $|\vec{k}+\rangle$ to $|\vec{k}'-\rangle$, simultaneously changing the impurity state from $|a\rangle$ to $|b\rangle$. Specifically,

$$\frac{dD}{dt} = 2\sum_{a,b}\sum_{\vec{k},\vec{k}'}\{W_{ab}(\vec{k}+, \vec{k}'-)N_a f_+(\vec{k})[1 - f_-(\vec{k}')] - W_{ba}(\vec{k}'-, \vec{k}+)N_b f_-(\vec{k}')[1 - f_+(\vec{k})]\}, \tag{A3}$$

where N_a is the number of scattering centers in state $|a\rangle$, and $f_+(\vec{k})$ is the Fermi function describing the nonequilibrium distribution of spin-up electrons. Here we have assumed that the nonequilibrium up- and

down-spin distributions can be characterized by the Fermi energies E_+ and E_-, respectively. Equations (A1) and (A3) can then be combined to provide a microscopic definition of T_1, and therefore of the TESR linewidth $\Delta H = 1/\gamma T_2$, since $T_1 = T_2$ in these systems when the Zeeman energies are small compared to kT.[43]

The exchange contribution to the linewidth is determined by setting

$$V(\vec{r}) = -(g_J - 1)J(\vec{r})\vec{J}\cdot\vec{s}\,. \tag{A4}$$

Then Eq. (A2) becomes

$$W_{ab}(\vec{k}+,\vec{k}'-) = (\pi/2\hbar)(g_J-1)^2|\langle b|J_+|a\rangle|^2[\,|J(\vec{k},\vec{k}')|^2/N_0^2]\delta(E_a + E_{\vec{k}+} - E_b - E_{\vec{k}'-})\,, \tag{A5}$$

where J_+, $J(\vec{k},\vec{k}')$, and N_0 are defined in the text. Putting this result into Eq. (A3) we obtain

$$\frac{dD}{dt} = \frac{\pi}{\hbar}(g_J-1)^2\sum_{a,b}|\langle b|J_+|a\rangle|^2\int\frac{\langle|J(\vec{k},\vec{k}')|^2\rangle_E}{N_0^2}\{N_a\rho_+(E)f_+(E)\rho_-(E-\Delta_{ba})[1-f_-(E-\Delta_{ba})]$$
$$-N_b\rho_-(E-\Delta_{ba})f_-(E-\Delta_{ba})\rho_+(E)\,[1-f_+(E)]\}\,dE\,, \tag{A6}$$

where $\langle|J(\vec{k},\vec{k}')|^2\rangle_E$ is defined as the average of $|J(\vec{k},\vec{k}')|^2$ over a surface of constant energy E, and the sum over $\vec{k},\vec{k}'$ has been converted to an integral in the usual way.[42] E is the total electron energy (kinetic + spin), $\rho_+(E)$ is the energy density of spin-up electron states per unit volume, and $\Delta_{ba} = E_b - E_a$. Note that the total energy conservation condition, $E' = E - \Delta_{ba}$, has been incorporated directly into this expression. To evaluate this integral we assume that the energy disturbance away from equilibrium is small ($E_- - E_+ \ll kT \ll E_F$), so that a first-order expansion of the Fermi functions in terms of this disturbance is a good approximation. We also assume that the impurity ions remain in thermal equilibrium (we neglect saturation and bottleneck effects), and that $\rho(E)$ and $\langle|J(\vec{k},\vec{k}')|^2\rangle_E$ are slowly varying functions of E. The result is

$$\frac{dD}{dt} = \frac{\pi}{\hbar}(g_J-1)^2(E_+ - E_-)\sum_{a,b}|\langle b|J_+|a\rangle|^2\int\frac{\langle|J(\vec{k},\vec{k}')|^2\rangle_E}{N_0^2}\,\rho_+(E)\rho_-(E-\Delta_{ba})(N_aN_b)^{1/2}$$
$$\times e^{-\beta\Delta_{ba}/2}\left(\frac{\beta e^{\beta(E-E_F)}}{(e^{\beta(E-E_F)}+1)(e^{\beta(E-\Delta_{ba}-E_F)}+1)}\right)dE$$
$$= \frac{\pi}{\hbar}(g_J-1)^2(E_+-E_-)\rho^2(E_F)\frac{\langle|J(\vec{k},\vec{k}')|^2\rangle_{E_F}}{N_0^2}N\langle G\rangle\,, \tag{A7}$$

where $\beta = 1/kT$, and $\langle G\rangle$ is defined in the text. Noting that $D - D_0 \cong \rho(E_F)(E_- - E_+)$, and defining $c = N/N_0$ and $\rho = \rho(E_F)/N_0$, Eqs. (A1) and (A7) combine to yield the expression for the exchange contribution to the TESR linewidth given by Eq. (2) in the text.

*Work supported by the U. S. Energy Research and Development Administration under Contract No. AT(11-1)-3150, Technical Report No. C00-3150-39. Additional support was received from the National Science Foundation under Grant No. GH-33637 through Cornell Materials Science Center, Report No. 2649.

†Present address: Varian Associates, 611 Hansen Way, Palo Alto, Calif. 94303.

‡Present address: Dept. of Physics, University of California, Los Angeles, Calif. 90024.

[1]R. B. Lewis and T. R. Carver, Phys. Rev. 155, 309 (1967), and references therein.

[2]S. Schultz, G. Dunifer, and C. Latham, Phys. Lett. 23, 192 (1966), and references therein.

[3]P. Monod and S. Schultz, Phys.Rev. 173, 645 (1968), and references therein.

[4]M. A. Huisjen, J. F. Siebert, and R. H. Silsbee, AIP Conf. Proc. 5, 1214 (1971).

[5]S. Schultz, D. R. Fredkin, B. L. Gehman, and M. R. Shanabarger, Phys. Rev. Lett. 31, 1297 (1973).

[6]Preliminary accounts have already appeared: J. F. Siebert, S. A. Dodds, and R. H. Silsbee, Arch. Sci. Genève 27, 239 (1974); Phys. Rev. Lett. 33, 904 (1974).

[7]P. M. Platzman and P. A. Wolff, in *Solid State Physics*, edited by F. Seitz and D. Turnbull (Academic, New York, 1973), Suppl. 13.

[8]J. R. Asik, M. A. Ball, and C. P. Slichter, Phys. Rev. 181, 645 (1969); 181, 662 (1969), and references therein.

[9]J. Owen, M. Browne, W. D. Knight, and C. Kittel, Phys. Rev. 102, 1501 (1956).

[10]The general problem of strongly coupled spin systems has been considered by many authors, a few of whom are listed here: D. C. Langreth and J. W. Wilkins, Phys. Rev. B 6, 3189 (1972); J. H. Pifer and R. T.

Longo, *ibid.* 4, 3797 (1971); M. B. Walker, *ibid.* 7, 2920 (1973).

[11]Space prohibits listing all references. See A. J. Heeger, in *Solid State Physics*, edited by F. Seitz and D. Turnbull (Academic, New York, 1969), Vol. 23, for a useful review.

[12]S. H. Liu, Phys. Rev. 121, 451 (1961).

[13]C. Rettori, D. Davidov, R. Orbach, E. P. Chock, and B. Ricks, Phys. Rev. B 7, 1 (1973).

[14]G. L. Dunifer, thesis (University of California, San Diego, 1968) (unpublished).

[15]M. A. Huisjen, thesis (Cornell University, Ithaca, New York, 1971) (unpublished).

[16]H. C. Theurer and J. J. Hauser, J. Appl. Phys. 35, 554 (1964); Trans. Metall. Soc. AIME (Am. Inst. Min. Metall. Pet. Eng.) 233, 588 (1965).

[17]N. L. Peterson and S. J. Rothman, Phys. Rev. B 1, 3264 (1970).

[18]J. R. Asik, thesis (University of Illinois, 1966) (unpublished); R. J. Elliot, Phys. Rev. 96, 267 (1954).

[19]M. Peter, J. Dupraz, and H. Cottet, Helv. Phys. Acta 40, 301 (1967).

[20]A. W. Overhauser, Phys. Rev. 89, 689 (1953).

[21]H. Hasegawa, Prog. Theor. Phys. 21, 483 (1959).

[22]Only the part of $1/T_{fs}$ that is linear in temperature is due to ground-state–conduction-electron cross relaxation. Other contributions to the observed rare-earth linewidth are due to higher crystal-field levels, which do not contribute to this cross relaxation. See L. L. Hirst, Phys. Rev. 181, 597 (1969).

[23]P. A. Wolff, Phys. Rev. 120, 814 (1960); 129, 84 (1963).

[24]A. Narath and H. J. Weaver, Phys. Rev. 175, 373 (1968).

[25]J. Zitkova-Wilcox, Phys. Rev. B 7, 3203 (1973). We would like to thank Dr. R. Orbach for pointing out this reference, and, in particular, for pointing out the need to include enhancement factors in the expression for the TESR linewidth.

[26]In determining the impurity contributions to the g value and linewidth of these alloys, we have referenced our data to TESR measurements made on pure Al over this same temperature range. Our results for pure Al are in agreement with those reported by D. Lubzens, M. Shanabarger, and S. Schultz [Phys. Rev. Lett. 29, 1387 (1972)].

[27]K. R. Lea, M. J. Leask, and W. P. Wolf, J. Phys. Chem. Solids 23, 1381 (1962).

[28]Because of this dependence and since our samples are polycrystalline, the computer calculations for the linewidth and g shift ought to be averaged over all field angles. However, numerical calculations indicate that the angular dependence of these quantities is small (less than 1%) if the splitting between the ground state and first excited state is more than 10 °K. Since the present data required splittings larger than 10 °K, we have simplified the calculations by choosing $\vec{H}$ along a fourfold axis.

[29]Y. Yafet (unpublished); see also J. Sweer, D. C. Langreth, and J. W. Wilkins, Phys. Rev. B 13, 192 (1976), and references therein.

[30]T. Plefka (private communication). The calculation is a generalization of that presented in T. Plefka, Phys. Status Solidi B 55, 129 (1973).

[31]G. Williams and L. L. Hirst, Phys. Rev. 185, 407 (1969).

[32]C. Rettori and E. P. Chock, Solid State Commun. 12, 621 (1973).

[33]S. Oseroff, D. Wohlleben, and S. Schultz (unpublished); S. Oseroff, B. Gehman, S. Schultz, and C. Rettori, Phys. Rev. Lett. 35, 679 (1975).

[34]M. B. Walker, Phys. Rev. 176, 432 (1968); R. Orbach and H. J. Spencer, *ibid.* 179, 690 (1969).

[35]Within experimental error these results agree with independent EPR measurements on Al: Er, as reported in Ref. 13.

[36]R. W. Reynolds, Y. Chen, L. A. Boatner, and M. M. Abraham, Phys. Rev. Lett. 29, 18 (1972).

[37]G. A. Matzkanin, J. J. Spokas, C. H. Sowers, D. O. Van Ostenberg, and H. G. Hoeve, Phys. Rev. 181, 559 (1969).

[38]We would like to thank Dr. R. Orbach for pointing out the need for making this approximation in determining the value for $\langle J(\vec{q})\rangle^2_{E_F}$.

[39]All measurements were made at 9.2 GHz and we have used the free-electron value $V_F = 2.0 \times 10^8$cm/sec in calculating these cross sections.

[40]S. A. Dodds, thesis (Cornell University, 1975) (unpublished).

[41]A. J. Dekker, J. Appl. Phys. 36, 906 (1965).

[42]C. P. Slichter, *Principles of Magnetic Resonance* (Harper and Row, New York, 1963), p. 89.

[43]Y. Yafet, in *Solid State Physics*, edited by F. Seitz and D. Turnbull (Academic, New York, 1963), Vol. 14.